



Multi-objective optimization of foam-filled tubes to enhance the crashworthiness characteristics under impact loading

Shubham Bhutada¹ · Saurabh Sonje¹ · Manmohan Dass Goel¹

Received: 15 April 2023 / Accepted: 28 July 2023 / Published online: 24 August 2023

© The Author(s), under exclusive licence to The Brazilian Society of Mechanical Sciences and Engineering 2023

Abstract

The study presents an understanding of the tube crushing behaviour modified with multiple geometrical configurations. Along with the foam-filling technique, the modifications in a tube geometry are configured in the form of multiple number and shapes of cut-outs. In order to understand the initial buckling behaviour, modified tube structures are subjected to impact loading using finite element (FE) numerical model of split-Hopkinson pressure bar (SHPB) apparatus. The FE analysis of tube deformation is carried out using ABAQUS/Explicit[®]. Later on, aluminium foam is filled in hollow tube structures with cut-outs to enhance its energy absorption capacity. Various crashworthiness parameters such as load–deformation profile, peak crushing load, crush load reduction, energy absorption capacity, and energy efficiency are computed and discussed. Tube deformation behaviour is studied on the basis of force transfer rate through the tubes. Tubes with diamond cut-outs are found to be having least force transfer rate value. Foam-filled tubes with cut-outs have shown excellent performance in terms of energy absorption capacity and energy efficiency. Approximately 80% of energy efficiency is achieved in the foam-filled tubes with cut-outs, which is nearly 36.7% and 42.37% higher than the foam-filled tube and hollow tubes without cut-outs, respectively. Moreover, the positive effect of interaction ratio has been observed between the tube and foam material.

Keywords Aluminium foam · Crashworthiness · Cut-outs · Energy absorption · Impact velocity · Interaction effect · Peak Load

1 Introduction

Tubes are used as an energy absorbing device in various field applications of automotive, aeronautical, and defence sector, where the structure and its components are subjected to high velocity impact conditions. This high velocity impact condition is observed during collision of vehicles, where large amount of kinetic energy is imparted to vehicle body, and the loading can be due to frontal, lateral, or oblique impact. Thin-walled tubes are considered to be of great importance during such collision events. These tubes have the ability to reduce the transfer of force along with the absorption of imparting kinetic energy on to the tube walls, either in axial, oblique, or lateral direction.

Thin-walled tubes have been explored as an energy absorbing device since 1960, owing to pioneers such as Pugsley and Macauley [1] and Alexander [2]. They understood the deformation mechanism of thin-walled tubes under axial loading phenomenon, and derived the empirical equations for the peak load and mean load bearing capacity of tubes. Later on, Andrews et al. [3] presented the classification of cylindrical tubes subjected to quasi-static axial loading and developed a classification chart for deformation modes of tubes on the basis of their L/D and t/D ratios. Many subsequent research papers have emphasized the importance of this categorization chart in determining tube geometry. Along with this chart, Abramowicz and Jones [4–7] invention of the half fold length formula has made a significant contribution to the research of axial crushing of thin-walled tubes. Reid [8] presented a comprehensive idea of the available research literature with detailed discussion on the deformation mechanisms of metal tubes used as energy absorbers under axial impact loading. Energy absorption characteristics are very crucial for the tubes subjected to dynamic loading. Sudden change in loading from quasi-static to dynamic

Technical Editor: João Marciano Laredo dos Reis.

✉ Manmohan Dass Goel
mdgoel@apm.vnit.ac.in

¹ Department of Applied Mechanics, Visvesvaraya National Institute of Technology, Nagpur 440 010, India

can change the overall material and deformation characteristics of tube. Accompanying to these changes in thin-walled tubular structures, many other factors like inertial effects, strain hardening effect, loading conditions, and stress wave propagation play a significant role in the research of thin-walled tubes subjected to dynamic loading. The effect of inertia, stress wave propagation, and loading pulse under dynamic elastic–plastic buckling of tubes is studied by Karagiozova et al. [9–14].

Other factors which can affect the loading and energy absorption characteristics of the tube include the different types of geometrical modifications which can be developed in the tube geometry. These modifications are mainly observed of 5 different types, i.e. chamfering (or indentations), corrugations (or grooves), external triggers, cut-outs, and multi-cell tubes [15].

In order to modify the tube deformation mode in a controlled manner and to maximize the enhancement of energy absorption capacity of tubes under axial loading, cut-outs in the tube geometry are found to be the most efficient type of geometrical modifications among all the others. Along with the reduction in tube weight, providing cut-outs in tube geometry helps in peak load reduction and controlling the deformation pattern of the tube. Gupta and Gupta [16] initially analysed the mild steel and aluminium tubular structures in as-received and annealed condition by providing cut-outs on the tube surface. They observed the reduction in peak load as well as the possibility of stabilizing the longer length tubes into stable deformation mode other than Euler buckling. Moreover, researchers [17–22] studied the effect of single cut-out on the tube surface at different locations and with different shapes of cut-outs like circular, square, rectangular, elliptical, and slotted type. One of the most common conclusions drawn by these research studies is the reduction in peak load value of tube with the deformation of tube into stable mode of collapse rather than deforming into global bending mode. Another group of researchers [23, 24] studied the effect of cyclic axial loading on the strain hardening behaviour and hysteresis loop characteristics of the material due to provision of single cut-out at different locations along the tube length. They concluded that the provision of the cut-out in tube smoothens the deformation behaviour of tube and increase in the size of cut-out significantly affects the hysteresis loop characteristics of tube material. Further, research work is carried out on the multiple number of cut-outs having square, circular, and elliptical shape and located at different locations along the length and circumference of a tube [25–28]. From these studies, the tube behaviour showed the reduction in peak collapse load along with the optimization in energy absorption capacity of tubes. Rouzegar et al. [29] performed quasi-static axial crushing on aluminium and composite wrapped aluminium tubes. These tubes were provided with multiple circular perforations on

the tube surface. Ozbek et al. [30] carried out crashworthiness analysis on GFRP composite pipes with different number and size of cut-outs. They concluded that as the size of cut-out increases, the peak collapse load of the composite pipes reduces significantly. Other researchers used different tube geometries and materials as well as different shape of cut-outs on the tube surface to optimize the load and energy absorption characteristics of the tubular structure [31–35].

Other than the above-mentioned geometrical modifications, filling of energy absorbing material into the thin-walled tubes is also been considered as the modification in the energy absorbing structure. Reid et al. [36] developed the composite structure of foam filled in the sheet metal tubes of mild steel material filled with polyurethane (PU) foam. The static and dynamic crushing of foam-filled sheet metal tubes showed a controlled deformation mode of crushing in long tubes. And, the interaction between foam and tube was studied with the help of theoretical formulae developed. Later on, researchers tried different techniques of filling the typical energy absorbing structures (i.e. tube structures, sandwich structures, etc.) with materials like PU foam, polyvinyl chloride (PVC) foam, aluminium foam, polymeric auxetic foam, agglomerate cork, and different geometric lattice structures, to enhance the crashworthiness characteristics like reduction in peak collapse load and increase in energy absorption characteristics [37–47].

Furthermore, the study on enhancement of tube behaviour and characteristics is carried out by providing multiple modifications in the tube geometry. Montazeri et al. [48] studied the behaviour of tube by implementing cut-outs and grooves on the surface of mild steel and aluminium tubes. These multiple modifications showed that the tubes with cut-outs behave with an enhanced crushing characteristic as compared to the tubes with grooves and tubes without any modifications. Goel [49] considered the multi-cell tubular structure for crashworthiness which showed the increase in energy absorption capacity of the structure. Estrada et al. [50] considered multi-cell tubular structures with cut-outs. Similarly, Pirmohammad and Esmaeili-Marzdashti [50] adopted the bi-tubular square and octagonal cross section tubes with cut-outs of square, hexagonal, elliptical shapes. This extensive study showed the enhancement of 60% and 42% in bi-tubular structure with hexagonal cut-outs as compared to the bi-tubular structures without cut-outs. Booth et al. [52] investigated the behaviour of multi-cell tubular structure with circular cut-outs on the tube surface which led to significant increase in the energy absorption characteristics. Sarkhosh et al. [53] experimentally investigated the behaviour of composite tubes filled with aluminium honeycomb and PU foam under quasi-static loading condition. The results of the investigation showed that composite tubes filled with both PU foam and aluminium honeycomb are able to deform into stable mode of collapse with the

significant increase in energy absorption characteristics due to infill materials. Moreover, study on behaviour of tubes with multiple modification was extended to the foam-filled tubular structures developed with geometrical modifications. Sarkabiri et al. [54] conducted a quasi-static multi-objective crashworthiness analysis on frusta cones by providing circumferential grooves on tube surface and filling of PU foam inside the modified tube geometry. Foam filling is observed to be improving the tube's deformation and crashworthiness characteristics [15]. Xie et al. [55] performed dynamic analysis on the AA 6063-T5 square tubes having multiple holes and filled with aluminium foam. The holes are distributed along the length of the tube on one side of the square tube. The results showed that provision of holes affects the load–deformation characteristics of the tube significantly and the effect of foam filling helps in enhancement of energy absorption.

Review conducted in the present study is based on the behaviour of tubular structures and the enhancement in their performance characteristics through implementing geometrical modifications and foam-filling technique. However, extensive research has been carried out and the structures were modified to a significant extent in many of the studies. But, the comparative crashworthiness study on tubes with different types of multiple cut-outs has not been conducted. Additionally, the placement or arrangement pattern of tube also plays a very crucial role in its deformation behaviour. Many researchers have tried to place the cut-outs on tube surface in a longitudinal direction. When it comes to different shapes of cut-outs, the effect of cut-out placement in circumferential pattern still remains unexplored. This study covers these research gaps by providing multiple modifications to the similar tube geometry of circular cross section as considered by Sankar and Parameswaran [27]. Sankar and Parameswaran [27] carried out a study on the buckling behaviour of stubby shells which led to the reduction in initial peak load value of tube structure with circular cut-outs. The present study is carried out by keeping the same modification criteria, the tubes are provided with square and diamond shapes of cut-outs on their surface and compared with the tubes having circular cut-outs [27]. Further, these tubes are filled with aluminium foam material to enhance the energy absorption characteristics of tubes with cut-outs. These tubular structures with multiple modifications are studied under the impact loading condition, using ABAQUS/Explicit® [56], to understand the behaviour of parameters like peak collapse load, crush load reduction, energy absorption capacity, and energy efficiency. These parameters are estimated for the 30% deformation length of the tube. Further, varying trend in slope behaviour of load–displacement profile and the interaction effect due to foam filling is also studied which helped in better understanding of the initial buckling behaviour of tube structure under impact loading

condition. Thus, the current work attempts to understand the initial buckling response of circular AA6061-T6 tubes subjected to axial impact loading by employing a multi-objective optimization technique with different cut-out configurations and filling aluminium foam in the modified tube geometry.

2 Specimen geometrical details

Aluminium alloy tubes of material grade 6061 and T6 temper and the infill of aluminium foam material are chosen for the current study. Geometry of tube material is circular in cross section with mean diameter of 14.5 mm, 0.5 mm thickness, and 10 mm length. As per Andrews et al. [3] classification chart for collapse mode of aluminium alloy tubes, if the L/D and t/D ratios of tube are approximately 0.6 and 0.03, then the tube is expected to collapse into concertina mode of deformation. This concertina mode of deformation is said to be the effective mode in terms of crashworthiness characteristics of tube. Further, the length of tube was kept as 10 mm such that after the complete collapse of tube under compression, it would be able to form a single complete fold for the understanding of its collapse characteristics. The calculation of tube length required for a one complete fold depends upon the thickness (h) and mean radius (R) of tube, and is calculated as per Eq. (1) given by Abramowicz and Jones [5] as under,

$$\frac{H}{R} = 1.73 \left(\frac{h}{2R} \right)^{1/2} \quad (1)$$

Here, ' H ' is the half fold length of the circular tube undergoing compression. The value of H comes out to be 4.66 mm and thus the length required for one complete fold would be approximately 10 mm. Further, the aluminium foam is considered as an infill material for the tube. The diameter and length of foam material will be same as the inner diameter and length of the tube, respectively. Figure 1 shows the geometrical illustrations of hollow tube and infill foam material.

The geometry of tubes is modified further by providing cut-outs on its surface. These cut-outs are varied in shape and size by keeping a constant weight reduction of 10% in each of the sample. Three different shapes of cut-out are chosen to control the deformation behaviour of tubes, as represented in Fig. 2c, d, and e. These shapes of cut-outs are provided over hollow tube (HP) and foam-filled tube (FP) as shown in Fig. 2a and b, which will produce 30 different configurations of tube specimens.

The shape and dimensions of cut-outs for the particular specimen along with its nomenclature are summarized in Table 1. The nomenclature of a particular specimen can be read as 'HP-C-2-12', where H or F in HP/FP stands for

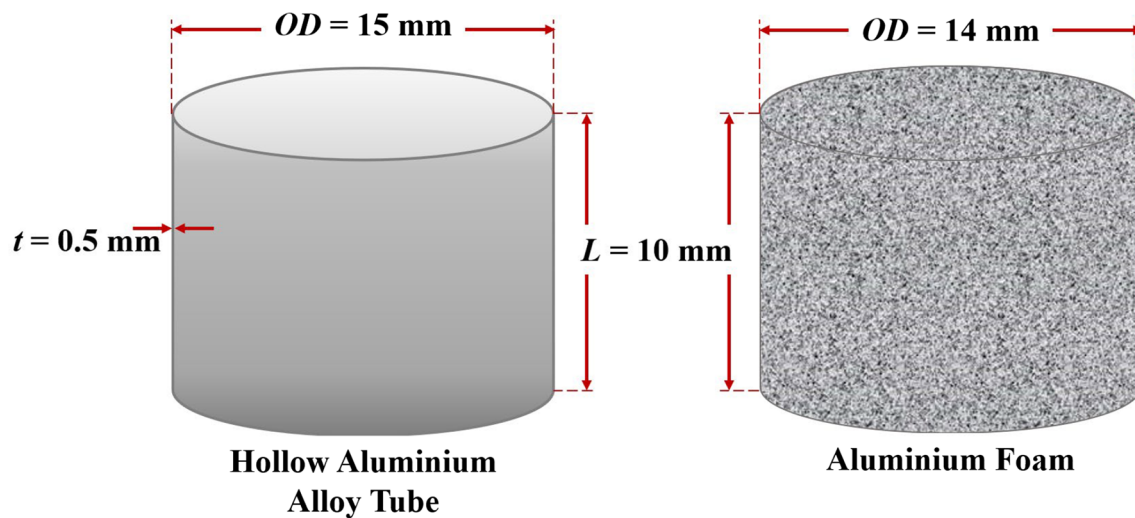


Fig. 1 Geometrical illustrations of hollow aluminium alloy tube (*T*) and aluminium foam (*F*)

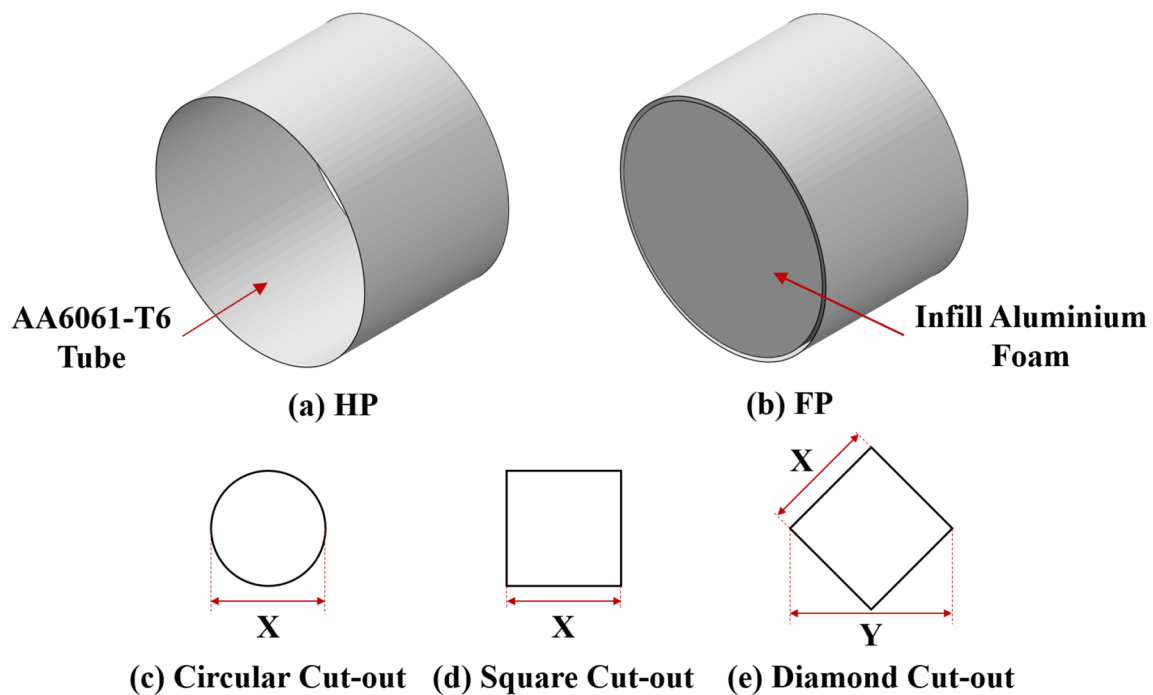


Fig. 2 Cut-out configurations for different tube specimens

hollow and foam-filled tubes, respectively. C/S/D stands for circular, square, and diamond shape of cut-outs, respectively. Number 2 stands for dimension 'X' of cut-out as shown in Fig. 2. Number 12 stands for number of cut-outs lying along the circumference of tube in a single line. The centre lines of cut-outs are provided at the mid-high level of tube, i.e. 5 mm from the end of tube.

Each of the specimen tabulated above is illustrated with the help of 3D model in Fig. 3. Here, the specimens are

divided mainly into 3 groups on the basis of cut-out shapes, i.e. circular, diamond, and elliptical. Each configuration of hollow tube is replicated as a foam-filled counterpart, as it is filled with aluminium foam throughout its length. For dynamic compression analysis, specimens are grouped together on the basis of equal weight reduction criteria and equal net section perimeter criteria.

Table 1 Nomenclature of specimen for different shape and size of cut-outs

Specimen nomenclature	Cut-out shape	Cut-out dimension (X) (mm)	Number of cut-outs	Mass (g)	Net circumference (mm)
HP	–	–	–	0.634	45.5
F	–	–	–	0.462	44.0
FP	–	–	–	1.096	45.5
HP-C-2-12*	Circular cut-out	2	12	0.570	21.5
HP-C-3-5*		3	5	0.573	30.4
HP-C-4-3*		4	3	0.569	33.4
HP-C-2-6*		2	6	0.605	33.5
HP-C-3-4*		3	4	0.597	33.5
FP-C-2-12		2	12	0.975	21.5
FP-C-3-5		3	5	0.981	30.5
FP-C-4-3		4	3	0.975	33.5
FP-C-2-6		2	6	1.026	33.5
FP-C-3-4		3	4	1.000	33.5
HP-S-2-12	Square cut-out	2	12	0.485	21.5
HP-S-3-5		3	5	0.493	30.5
HP-S-4-3		4	3	0.485	33.5
HP-S-2-6		2	6	0.550	33.5
HP-S-3-4		3	4	0.518	33.5
FP-S-2-12		2	12	0.947	21.5
FP-S-3-5		3	5	0.955	30.5
FP-S-4-3		4	3	0.947	33.5
FP-S-2-6		2	6	1.012	33.5
FP-S-3-4		3	4	0.980	33.5
HP-D-2-12	Diamond cut-out	2	12	0.485	11.6
HP-D-3-5		3	5	0.493	24.3
HP-D-4-3		4	3	0.485	28.6
HP-D-2-6		2	6	0.550	28.6
HP-D-3-4		3	4	0.518	28.6
FP-D-2-12		2	12	0.947	11.6
FP-D-3-5		3	5	0.955	24.3
FP-D-4-3		4	3	0.947	28.6
FP-D-2-6		2	6	1.012	28.6
FP-D-3-4		3	4	0.980	28.6

*Values are taken directly from the literature of Sankar and Parameswaran[27]

3 Finite element modelling and simulation

The present study carries out dynamic explicit analyses on tube specimens under compression using ABAQUS/Explicit®. Split-Hopkinson pressure bar (SHPB) is used to analyse the dynamic compressive behaviour of materials under high strain rates (10^2 – 10^4) [57]. The incident and transmitter bars are used to create a FE model of the SHPB, and the tube specimen is dynamically compressed between these two bars. The incident bar is initially dynamically loaded with the help of a high velocity impacting striker. This impact will generate a stress wave to go from one end of the incident bar to the other. The incident bar's opposite

end is in contact with the specimen. As a result, the stress wave travelling through the bar will be partially transferred into the specimen, with the remainder being reflected back into the incident bar. The stress wave that strikes the specimen is referred to as the incident wave (ϵ_I), and the wave that is reflected back is referred to as the reflected wave (ϵ_R). The transmitted wave (ϵ_T) will be the stress wave that enters the transmitter bar via the bar-specimen contact, after the specimen is unloaded. The testing section of the SHPB is shown in Fig. 4, where the incident wave impacts on the specimen, and part of this incident wave is reflected back, while the other part is transmitted through the specimen into transmitter bar. During the loading stage, the specimen

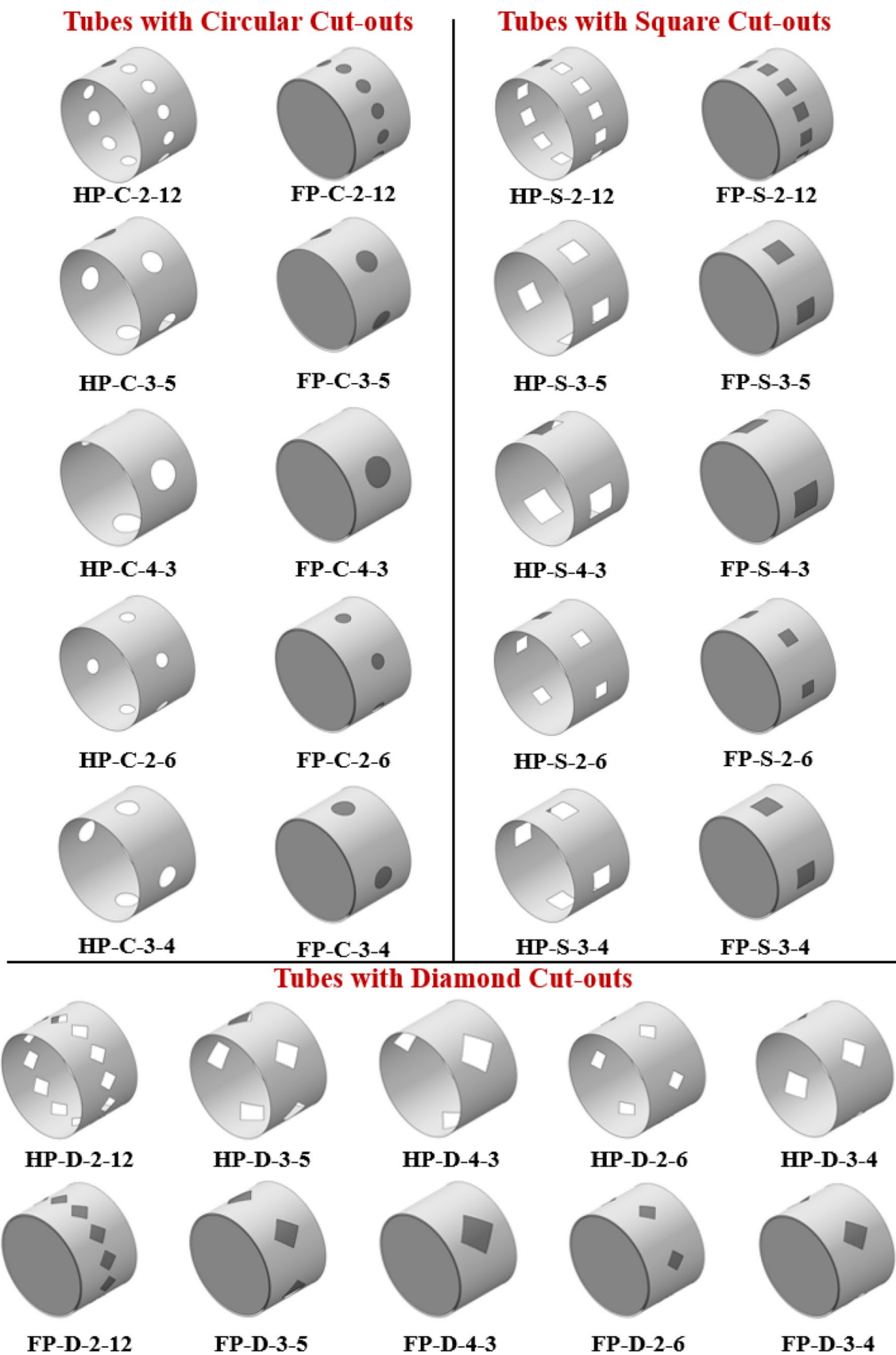


Fig. 3 Tube specimens with different cut-out configurations considered in the present study

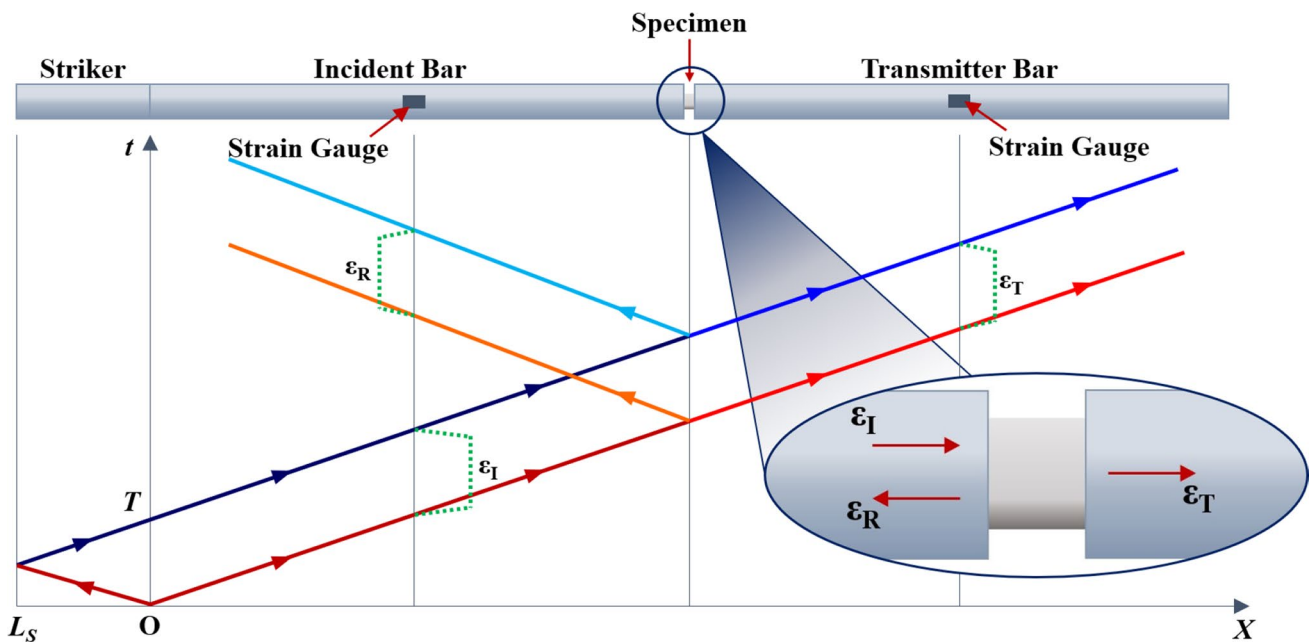


Fig. 4 Stress wave propagation in SHPB apparatus using X-t diagram—a schematic representation

will experience dynamic compression. This causes the tube specimen's dynamic buckling behaviour. In order to exactly simulate the aforementioned event, the present SHPB FE model is developed.

Moreover, Fig. 4 shows the schematic illustration of X-t diagram during a stress wave propagation in SHPB bars. X-t diagram correlates the stress wave propagation as an estimation of stress at any point X along the bar length at a given time t. This diagram helps to keep a track on the movement of stress wave in the SHPB system.

3.1 FE modelling details

Incident and transmitter bars in SHPB apparatus are defined as linearly elastic solid homogeneous bars with an 8-noded C3D8R linear solid brick element. The incident bar is kept long enough, up to 3000 mm, to eliminate wave dispersion caused by reflected waves from the bar-specimen contact. The length of the transmitter bar, on the other hand, is modelled as 2000 mm. Each bar has a diameter of 20 mm. The linearly elastic bars are made of aluminium alloy 7075-T6 with a Young's modulus of 70 GPa and a Poisson's ratio of 0.3. An elastic–plastic homogeneous shell element is used to simulate the cylindrical hollow tube. This entire shell section is represented by a 4-noded S4R reduced integration element with 5 integration points along its thickness. The tube is made of aluminium alloy 6061-T6 grade. In ABAQUS/Explicit®, the Johnson–Cook material model [58] is employed to account for the material's strain rate

sensitivity. The von-Mises flow stress in the material is defined by the constitutive model as,

$$\sigma = [A + B\epsilon^n][1 + C \ln \dot{\epsilon}^*][1 - T^{*m}] \tag{2}$$

where A, B, and C are the parameters related to yield strength, strain hardening, and strain rate hardening of the material, respectively. n and m are the strain hardening and temperature softening exponent, respectively. T* is the homologous temperature at the reference strain rate, $\dot{\epsilon} = 1$. The values of these material model parameters for AA6061-T6 material are referred from [27], as mentioned in Table 2.

The aluminium foam filled in tubes is modelled using the crushable foam plasticity model with a material density of 300 kg/m³. The material is modelled as isotropic, elastic–plastic, and volume hardening model. The yielding behaviour of the foam material is governed by the yield surface in the p-q plane. This p-q plane is defined in between pressure stress and Mises equivalent stress, as shown in Fig. 5. The yield surface of material in initially governed by the ratios σ_c^0/p_c^0 and p/p_c^0 . The ratio σ_c^0/p_c^0 defines the ratio of initial yield stress of material under uniaxial compression to hydrostatic compression. The ratio p/p_c^0 defines the ratio

Table 2 Material model parameters for AA6061-T6 alloy material [27]

Parameter	A (MPa)	B (MPa)	n	C	m
Value	324	114	0.42	0.002	1.34

of yield stress in uniaxial tension to the initial yield stress in hydrostatic compression [56]. The properties of the parameters used to model foam are tabulated in Table 3 below.

The curve depicted in Fig. 6 defines the strain hardening behaviour of foam material under uniaxial compression. This curve is separated into three parts: the linear elastic zone, the plastic collapse region, and the densification region. The linear elastic zone concludes at a material yield point. The plateau region where the cells of foam deform plastically, compact, and begin to collapse with a very gradual increase in stress is known as the plastic collapse region. The cells of

compacted foam material collapsed completely in the densification zone, and the material densified even more.

To offer smooth sliding of tube folds over each other, boundary conditions are provided in the form of general contact to the tube section itself as frictionless. To induce tangential contact behaviour between the surfaces of the bar and the specimen, a frictional coefficient of 0.25 is introduced between them. This will aid in the proper transfer of force between the bars and specimen, as well as preventing one face from sliding over another [12]. The incident bar's end face in contact with the specimen receives an impact velocity of 9 m/s. Figure 3 depicts finite element (FE) simulations

Fig. 5 Yield surface in p - q plane of crushable foam model [56]

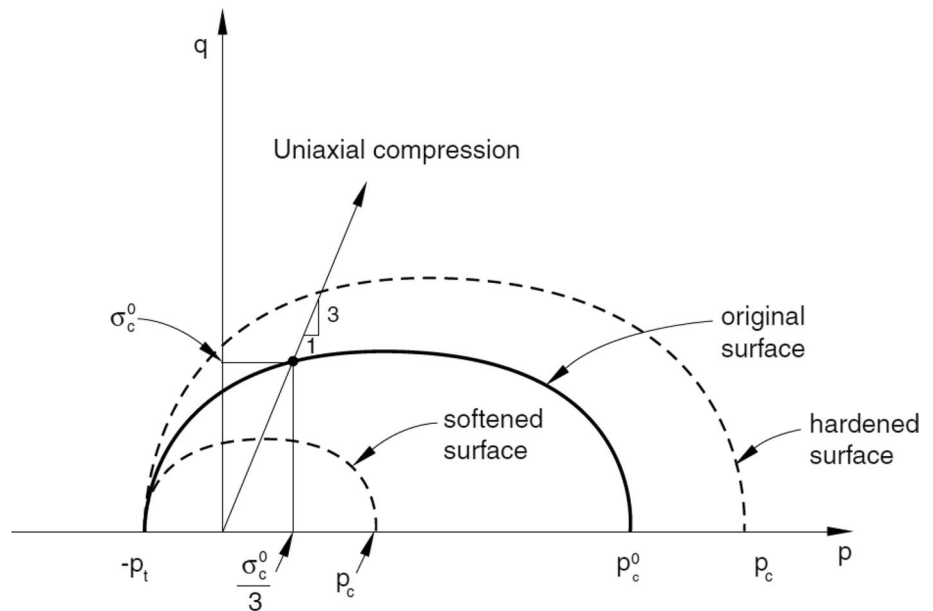
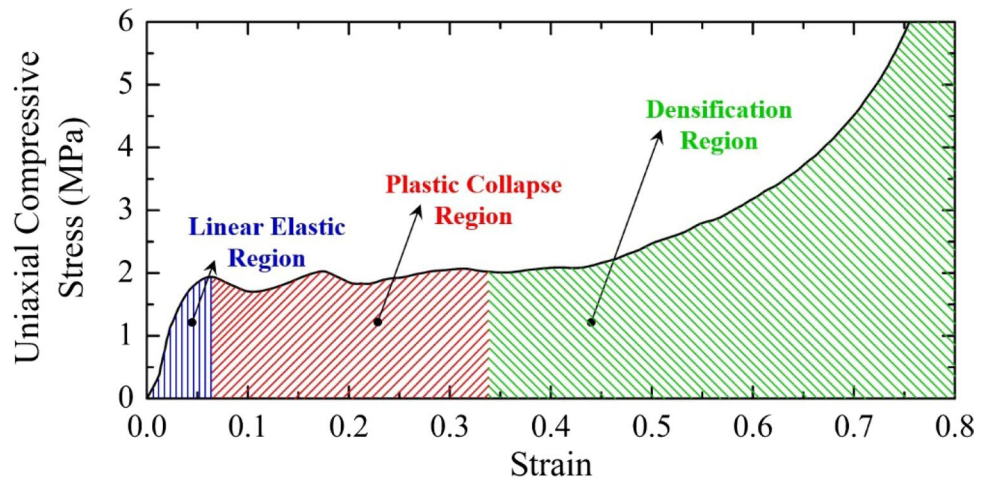


Table 3 Material model parameters for aluminium foam material [59]

Parameter	Density (kg/m ³)	Young's modulus (MPa)	Poisson's ratio	Yield stress (MPa)	σ_c^0/p_c^0	p/p_c^0
Value	300	5.0	0.0	2.2	1.72	0.16

Fig. 6 Stress-strain behaviour of aluminium foam material [59]



of hollow and foam-filled tube samples with varying shapes and dimensions of cut-outs. A mesh convergence study was carried out in order to arrive at a specific mesh size, which resulted in improved accuracy in results. To maintain the aspect ratio of each element, each tube sample is modelled with a mesh size of 0.2 mm. Furthermore, mesh size is optimized in the vicinity of cut-outs to control distortion of elements near cut-outs.

3.2 FE validation

In order to present the validation of FE model, the model of tube specimen without any cut-out is referred from the literature of Sankar and Parameswaran [27]. They have performed the experimental test on tube without cut-out subjected to impact velocity of 9 m/s. In this study, the FE model of similar setup is prepared as shown in Fig. 4, to test the similar specimen of tube without cut-out. The geometrical and material properties of the tube are considered similar to the referred literature. After obtaining the results and plotting the stress vs strain graph as shown in Fig. 7, the results of present FE model are observed to be in well agreement with

the results from literature of Sankar and Parameswaran [27]. The parametric values of the model are compared with the given experimental values from the literature of Sankar and Parameswaran [27], and significant agreement is found between the values tabulated in Table 4. The peak stress (σ_{max}) value of referred experiment results and present simulation results is having an agreement of 97.72%. Further, the deformed shape of tube is also represented in the inset of Fig. 7, for comparison in experimental and numerical model results. The deformed images are almost identical to each other. Thus, the present FE model can be said to be validated.

4 Results and discussions

Numerical investigation is carried out in the present study to understand the behaviour of hollow and foam-filled tubes under impact loading condition. This behaviour is studied with the help of load–deformation characteristics of the tube with different geometrical modifications. The deformation of tube is studied by determining the slope of load–deformation

Fig. 7 Validation of present FE results with the experimental results of Sankar and Parameswaran [27]

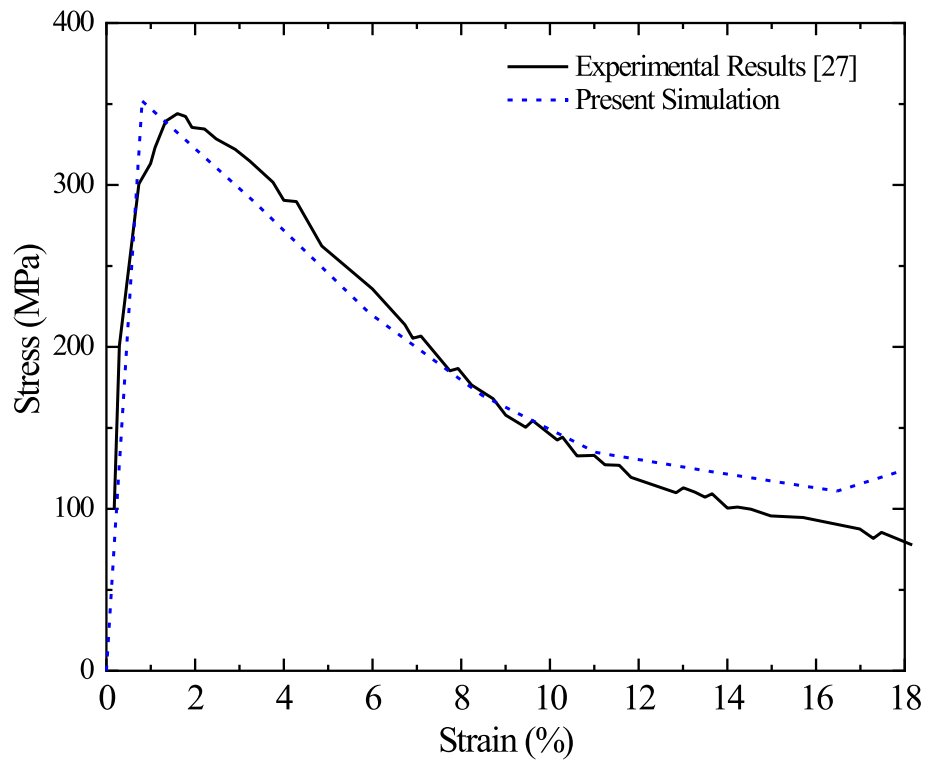


Table 4 Comparison of parametric values for validation

	Type of tube	σ_{max} (f_{max}) MPa (kN)	$E_{absorbed}$ (J)	η_{energy} (%)	SEA (kJ/kg)
Experimental results [27]	P_s	344 (7.8)	11.26	47.9	17.9
Present simulation	P	352 (8.0)	12.13	52.1	19.7

Table 5 Characteristics values of hollow and foam-filled tubes without cut-outs and bare foam specimen

Tube specimen	Peak load (F_{peak}) (kN)	Energy absorbed ($E_{absorbed}$) (J)	Energy efficiency (η_{energy}) (%)
HP	8.02	13.4	55.7
Bare foam	0.23	0.26	37.8
FP	8.15	14.2	58.0

curve of a tube specimen. Furthermore, energy absorption characteristics of the tube specimens are studied to optimize the geometrically modified tube. The energy absorbed by tube and foam separately and the energy absorbed by foam-filled tube is used to study the interaction effect between tube and foam material. To keep the consistency in analysis of FE simulation results, tube deformation length (δ) has been restricted to 30% of the original tube length. Each simulation

is carried out under the impact velocity of 9 m/s. The above-mentioned output parameters are obtained from the numerical simulations and tabulated in Tables 5, 6 and 7 for hollow and foam-filled tube specimens without cut-outs and with circular, square, and diamond cut-outs, respectively. Peak load (F_{peak}) value for each tube specimen in Tables 5, 6 and 7 is taken as the maximum load bearing capacity of each specimen before it starts to deform itself into fold. Crush load reduction ($F_{reduced}$) is calculated as the percentage ratio of decrease in the peak load value for the specimen with cut-out to the peak load value of tube specimen without cut-out. For hollow tubes, the comparison is made between the hollow tubes with and without cut-out specimens. Similarly, for foam-filled tubes, the comparison is made between the foam-filled tubes with and without cut-out specimens. Energy absorbed by the specimen is calculated as the area under load–displacement curve of that specimen. Energy efficiency is estimated as the percentage ratio of actual

Table 6 Characteristics values of hollow and foam-filled tubes with circular cut-outs

Tube specimen	Peak load (F_{peak}) (kN)	Crush load reduction ($F_{reduced}$) (%)	Energy absorbed ($E_{absorbed}$) (J)	Energy efficiency (η_{energy}) (%)
<i>Cut-out modification criteria: equal mass reduction</i>				
HP-C-2-12*	4.50	42.3	9.2	68.0
HP-C-3-5*	5.30	32.9	8.7	55.0
HP-C-4-3*	5.50	29.7	8.5	51.2
FP-C-2-12	4.88	39.2	10.1	69.3
FP-C-3-5	5.82	27.3	10.3	59.2
FP-C-4-3	5.77	28.0	9.8	56.5
<i>Cut-out modification criteria: equal net circumference</i>				
HP-C-2-6*	6.20	21.2	10.3	55.4
HP-C-3-4*	5.80	26.2	9.5	54.8
FP-C-2-6	6.12	23.7	11.7	63.6
FP-C-3-4	6.24	22.2	11.1	59.3

*Values are taken directly from the literature of Sankar and Parameswaran[27]

Table 7 Characteristics values of hollow and foam-filled tubes with square cut-outs

Tube specimen	Peak load (F_{peak}) (kN)	Crush load reduction ($F_{reduced}$) (%)	Energy absorbed ($E_{absorbed}$) (J)	Energy efficiency (η_{energy}) (%)
<i>Cut-out modification criteria: equal mass reduction</i>				
HP-S-2-12	4.29	46.54	9.4	73.4
HP-S-3-5	5.08	36.67	8.3	54.6
HP-S-4-3	5.74	28.37	8.9	51.5
FP-S-2-12	4.50	43.81	10.7	79.3
FP-S-3-5	5.65	29.55	8.7	51.5
FP-S-4-3	5.74	28.40	9.6	55.6
<i>Cut-out modification criteria: equal net circumference</i>				
HP-S-2-6	5.87	26.72	10.8	61.5
HP-S-3-4	5.56	30.59	9.4	56.5
FP-S-2-6	6.05	24.53	11.4	62.7
FP-S-3-4	5.89	26.56	10.1	57.5

energy absorbed by the specimen to the theoretical energy (i.e. $F_{peak} \cdot \delta$) absorbed by the specimen undergoing deformation. The effect of shape and size of cut-outs on each parameter is discussed in detail in further sub-sections.

4.1 Load–deformation characteristics

The load–deformation characteristics of a tube are crucial for examining the axial crushing behaviour of tubes under impact loading. For the current investigation on single fold formation in tube, peak load (F_{peak}), reduction in peak load ($F_{reduced}$), and the tube deformation behaviour are studied. Peak load is the maximum load carrying capacity of the tube subjected to impact. Peak load reduction is the difference between the peak load value of tube without cut-outs and the peak load value of tube with cut-outs, in terms of percentage. Deformation behaviour of tube is studied by observing the gradual decrement in the load value after reaching the peak. After reaching the peak load, if the load value decreases suddenly then it will cause a significant jerk transferring at the far end of the tube (other than impact end). Thus, the gradual decrement in load value will lower the jerks coming onto the far end of tube, and it will transfer the load smoothly which is a requirement of an effective crashworthiness component.

4.1.1 Load bearing characteristics of tube

Figure 8a shows the graphical representation of load–displacement profile for the hollow and foam-filled tubes with circular cut-outs. The results of hollow tube with circular cut-outs configuration are taken from the numerical work carried out by Sankar and Parameswaran [27]. Further, these similar tubes are filled with an aluminium foam material to efficiently control the deformation of tubes

with absorption of high amount of energy. However, the load–deformation characteristics of foam-filled tubes show higher peak load value as compared to the peak load value of their hollow counterparts. But the energy absorption of foam-filled tubes is observed to be higher than hollow tubes. The HP-C-2-12 tube configuration was observed to be the most efficient cut-out configuration among all the others in case of equal weight reduction criteria [27]. When these tubes are filled with aluminium foam, they showed approximately 5–9% of increase in peak load value and 9–16% of increase in energy absorption value than the hollow tubes. Among the tubes with equal mass reduction criteria in Table 6, the FP-C-3-5 configuration gives the highest energy absorption value of 10.3 kJ. However, the same configuration also yields the highest peak load value of 5.82 kN. Another tube configuration among these criteria, i.e. FP-C-4-3 yielded the least increment in peak load value of 5.77 kN. This peak load value of foam-filled tube is only 4.7% higher than its hollow tube configuration, whereas the energy absorption value is observed to be increased by 13.26%.

Further from Table 6, on comparing the hollow and foam-filled tubes among equal net circumference criteria, three configurations are to be compared, i.e. HP-C-2-6, HP-C-3-4, and HP-C-4-3. These configurations are compared with their foam-filled tube configurations, i.e. FP-C-2-6, HP-C-3-4, and HP-C-4-3. Among all the six tubes, the increase in peak load and energy absorption values of foam-filled tubes is 1–7% and 12–15%, respectively, as compared to that of hollow tubes as shown in Table 6.

Apart from the peak load value, load–deformation curve in Fig. 8a and b shows the complete deformation behaviour of tube to form a single fold over the complete tube length. This formation of fold is due to the absorption of kinetic

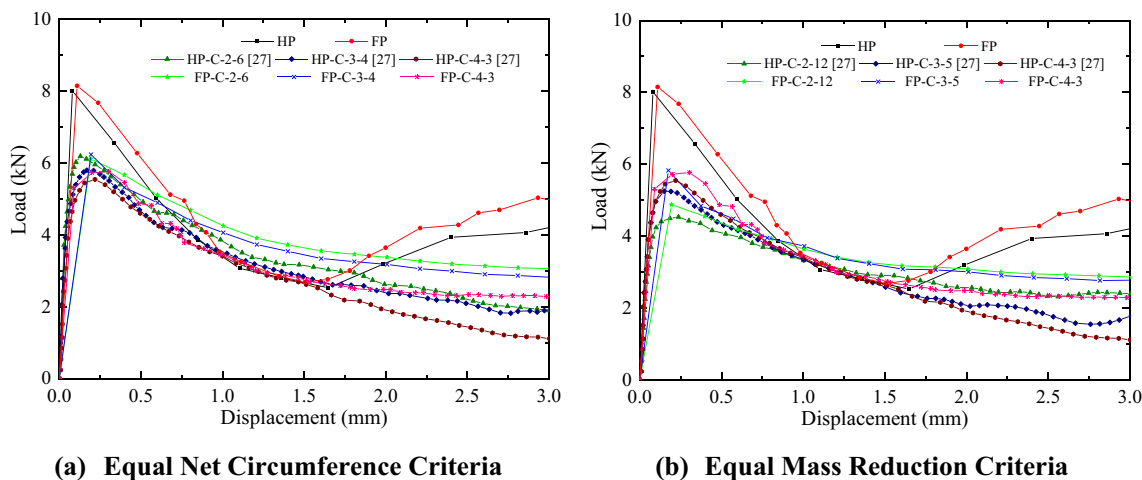


Fig. 8 Load–displacement profile of hollow and foam-filled tubes with circular cut-outs **a** equal net circumference criteria, and **b** equal mass reduction criteria

energy generated due to the transfer of force applied at the time of impact. From Fig. 8a, FP-C-2-6 specimen shows the largest area covered under the curve, i.e. highest energy absorption capacity as compared to other modified specimen results. Similarly, from Fig. 8b, FP-C-3-5 tube specimen covers the largest area under the curve and absorbs maximum kinetic energy at the time of impact as compared to other tube specimens in equal mass reduction configuration. The increase in peak load value of foam-filled tubes is due to the presence of larger material availability in the tube's cross section, which transfers the load on to the far end. Larger the material area available across the particular cross section of tube, higher will be the peak load value getting transferred to the far end. Thus, the peak load values are observed to be higher for foam-filled tubes in Fig. 8a and b.

Similar to Fig. 8a and b, the load–displacement characteristics are plotted in Figs. 9a and b, and 10a and b, for two different shapes of cut-outs on the tubes surface, i.e. square and diamond shape. Similar nature of observations is recorded for the square as well as diamond shape cut-outs. While taking observations from Fig. 9a and b, the 2 mm square cut-out tubes, i.e. the smallest size of cut-outs have shown the most efficient energy absorption capacity than other square cut-out tube, in both the hollow and foam-filled cases.

The hollow tubes with square shape cut-outs have obtained less value of peak load in all the tube configurations as compared to that of hollow tubes with circular shape cut-outs. In Table 7, tubes with square cut-outs for equal mass reduction criteria, the reduction in peak load is higher for HP-S-2-12 and HP-S-3-5 as compared to HP-C-2-12 and HP-C-3-5 hollow tubes with circular cut-outs, respectively. HP-S-2-12 tube configuration is found to be having the highest amount of peak load reduction among all the

tube configurations. This peak load reduction is 46.85% as compared to tube HP without any cut-outs. Further from the results tabulated in Table 7, foam-filled tubes with square cut-outs are observed to be having slightly lesser reduction in peak load value as compared to their counterparts in hollow tubes with square cut-outs.

Figure 10a and b shows the load–displacement profiles of hollow and foam-filled tubes with diamond shape cut-outs. The curve profile is similar to that of earlier configurations of circular and square cut-outs. However, the peak load value and the reduction in peak load value as compared to that of tube without any cut-outs makes a significant impact on the geometry of structure. After comparing the peak load values of HP-C-2-12, HP-S-2-12, and HP-D-2-12 tubes from Table 8, the tube configuration of HP-S-2-12 yielded the highest reduction in peak load, followed by HP-D-2-12 and HP-C-2-12. The difference between peak values of HP-S-2-12 and HP-D-2-12 is estimated to be 4.6%, and the difference between peak values of HP-S-2-12 and HP-C-2-12 is found out as 9.8%. The difference between the peak values changes significantly as soon as the shape of cut-out, i.e. the distribution area of cut-out changes. Thus, it can be said that the distribution area of cut-out plays a very significant role in the reduction of peak load value of the tube under deformation subjected to impact.

Further, other than peak load reduction Fig. 10a and b illustrates the area under load–displacement curve for each of the tube specimens with diamond cut-outs. Among these specimens, tubes with 2 mm of diamond cut-outs are observed to be the most efficient with larger area under the curve, i.e. higher energy absorption capacity as compared other cut-out modified tubes. Moreover, on comparing the foam-filled diamond cut-out tubes with foam-filled circular and square cut-out tubes, the configuration of FP-D-2-12

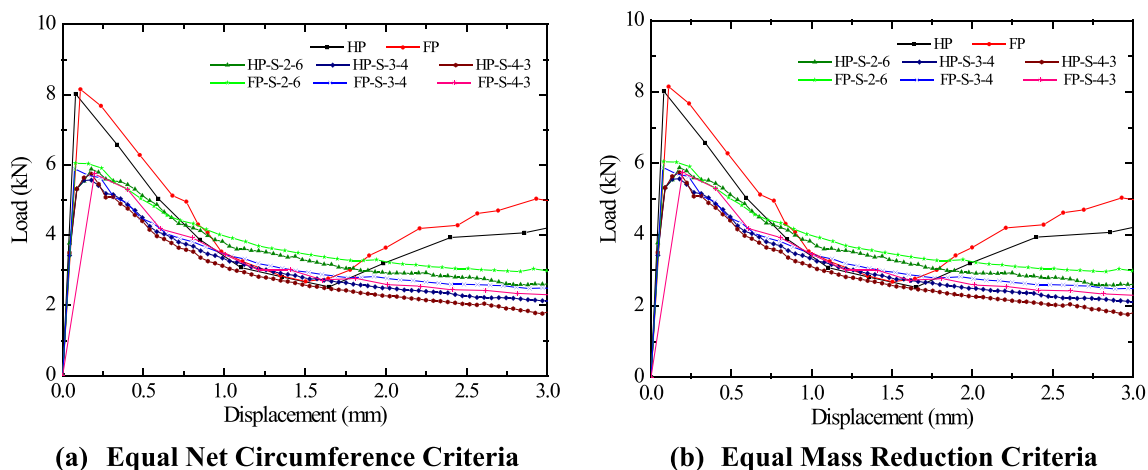


Fig. 9 Load–displacement profile of hollow and foam-filled tubes with square cut-outs **a** equal net circumference criteria, and **b** equal mass reduction criteria

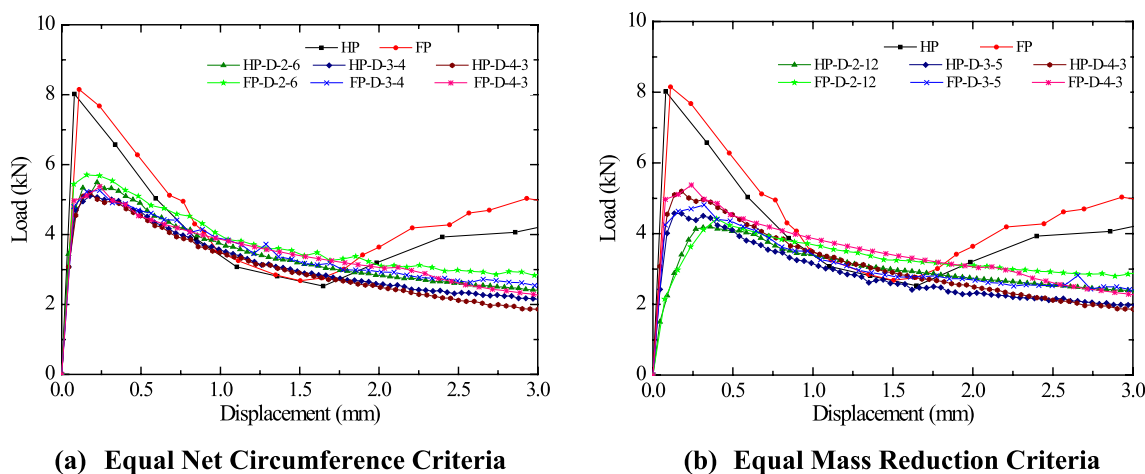


Fig. 10 Load–displacement profile of hollow and foam-filled tubes with diamond cut-outs **a** Equal Net circumference criteria, and **b** equal mass reduction criteria

Table 8 Characteristics values of hollow and foam-filled tubes with diamond cut-outs

Tube specimen	Peak load (F_{peak}) (kN)	Crush load reduction ($F_{reduced}$) (%)	Energy absorbed ($E_{absorbed}$) (J)	Energy efficiency (η_{energy}) (%)
<i>Cut-out modification criteria: equal mass reduction</i>				
HP-D-2-12	4.19	47.69	9.1	72.6
HP-D-3-5	4.57	42.95	8.6	62.5
HP-D-4-3	5.20	35.14	9.3	59.6
FP-D-2-12	4.42	44.84	10.0	75.4
FP-D-3-5	4.82	39.93	9.1	62.9
FP-D-4-3	5.37	32.94	10.2	63.3
<i>Cut-out modification criteria: equal net circumference</i>				
HP-D-2-6	5.49	31.47	10.4	62.9
HP-D-3-4	5.10	36.35	9.6	63.0
FP-D-2-6	5.70	28.86	11.5	67.0
FP-D-3-4	5.26	34.33	10.6	67.3

observed to be having least peak load value of 4.40, which made the peak load reduction of 45.15%. This value of peak load reduction was only 3% higher than that of FP-S-2-12, and 13.2% higher than that of FP-C-2-12.

Tubes with square shape cut-outs have offered the most optimized crashworthiness characteristics among all the tested specimens in the present study. The difference in peak load values and slope values in case of square and diamond cut-out tubes is negligible. Both the cut-out tubes, i.e. square and diamond cut-out tubes, have out-performed the circular cut-out tubes. However, the distribution of area in the vicinity of cut-out also plays a major role in deciding the value of peak bucking load of tube specimen. This has been mentioned and explained in Sect. 4.1.1 of the revised manuscript. The area between two subsequent cut-outs can be termed as critical area (CA) where the formation of fold takes place, as shown in figure below for tubes with different

shapes of cut-outs. The critical area is least in case of square cut-outs than circular and diamond cut-outs. Smaller critical area would offer lower resistance against load and would lead to an early deformation. Thus, the tube with square cut-outs showed higher strain accumulation in its cut-out vicinity leading to early initiation of tube deformation which can be observed from the slopes of load–displacement profile for these tubes (Fig. 12 of revised manuscript). The second aspect corresponds to the shape of critical region. Studies have reported that sharp corners cause higher strain accumulation and are the reason for the initiation of failure in the structures [60]. This further justifies the observation where circular cut-out tube shows higher peak load than diamond cut-out tubes and least peak load is obtained in square shape cut-out tubes in addition to its gradual decrease in load–displacement curve profile. Since square cut-out tubes accumulate more strain after the crash, they absorb kinetic energy

considerably sooner than the diamond and circular cut-out tubes, thus in turns reducing the transfer of force at the other end of tube (Fig. 11).

4.1.2 Discussion on the slope of load–displacement curve

When the tube undergoes deformation due to impact load, the developed load–displacement profile for the tube can be as shown in Fig. 12. Point A on the profile curve shows the peak load value or the peak load bearing capacity of the tube. Beyond point A, the impact load applied on the tube is getting converted into work done by tube in deforming itself in the form of folds. When the tube starts to develop folds, the value of load decreases. This value goes on decreasing until the formation of first half fold. Again, the curve starts to rise to complete the first fold formation. In case of normal tubes without cut-outs, it is observed that the load

value decreases sharply after reaching the tube’s load bearing capacity. However, in case of tubes with cut-outs, two significant points are observed. First, the peak load value of the tube decreases significantly as compared to peak load value of tube without cut-outs. Second, unlike in the case of tube without cut-outs, the load value in tubes with cut-outs decreases gradually after reaching its peak load value. To study the decreasing rate of curve, the slopes of different curves generated for different tube configurations are studied. Figure 12 represents the slope of load–displacement profile where $1/X$ is the slope of curve between points A and G. The value of X is obtained by averaging the slope between all the intermediate points. For example, slope X_{B-C} is the slope between points B and C of the curve profile. Similarly, the slope values of X_{A-B} , X_{C-D} , X_{D-E} , X_{E-F} , X_{F-G} are obtained and by averaging these slopes the value of X can be obtained. As the value of X decreases, the drop in the

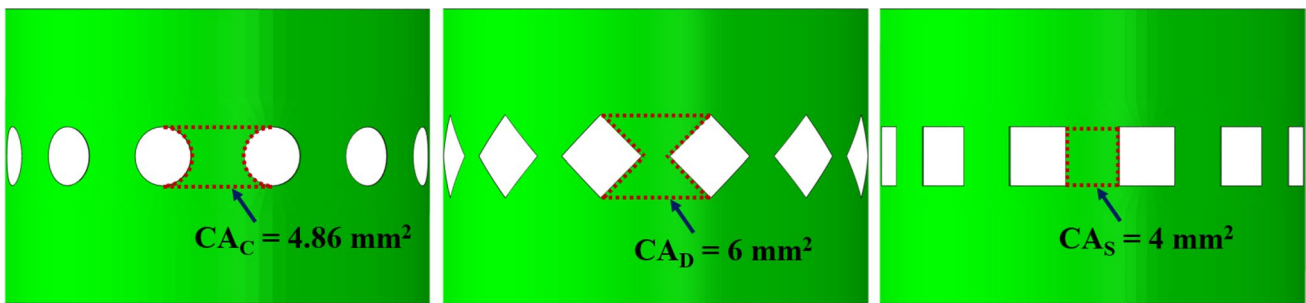
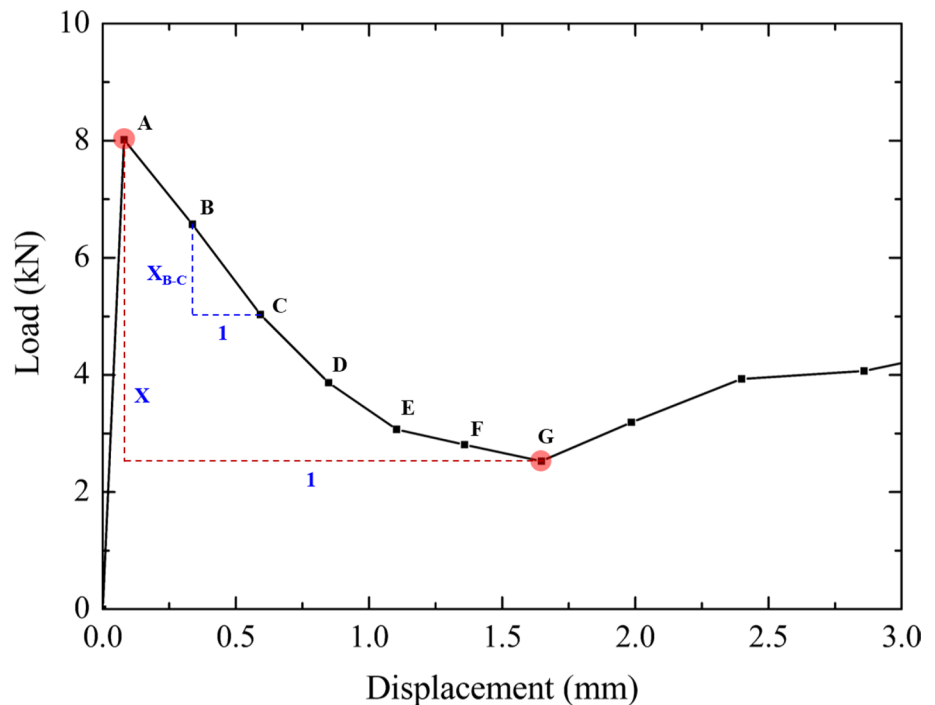


Fig. 11 Critical area region in tube specimens with each shape of cut-out

Fig. 12 Typical load–displacement profile of HP tube



curve decreases and the load value will decrease gradually. If the value of X increases, the drop in the curve increases and the load value will decrease rapidly.

The sudden drop in the load value in between the first half fold and second half fold (or in between any subsequent folds) will transfer the jerks to far end of the tube. This jerk at the far end of tube can be taken by any object attached on to that end of tube. For example, if the tube is used in vehicle’s frontal crash frame, the jerk will get transferred to the vehicle body, engine, or the occupant cell. This can lead to harmful injuries and fatalities to the occupants inside the vehicle. Thus, to reduce the amount of jerk on the far end of tube, the slope of the load–displacement curve should decrease gradually following the uniform and minimum load transfer condition. Thus, the value of X in the slope of 1 in X should be minimum, indicating the gradual rate of decrease in peak load value.

Figure 13 (a) and (b) represents the trend in variation of slope for each of the tube configurations presented in the study. Figure 13 (a) shows the tube specimens with the cut-out modification criteria of equal mass reduction. Here, the foam-filled tubes with diamond shaped cut-outs are found to be having least value of slope (X) for each size of cut-out configuration, owing to significant reduction in the slope of curve. Another trend can be seen in Fig. 13 (a), as the size of cut-out increases the slope value (X) rises, and the load–displacement profile becomes more critical.

Further, Fig. 13 (b) shows the trend in variation of slope values for the tubes with cut-out modification criteria of equal net circumference. The tubes in this configuration criteria show a nearly constant values for different size of cut-outs. Similar to Fig. 13 (a), foam-filled tubes with diamond shape cut-outs have shown least values of slope for the curves of each size of cut-outs.

However, on comparing Fig. 13 (a) and (b), the least slope value is obtained for FP-D-2-12 tube configuration. From Table 8, the peak load value for this tube configuration is obtained as 4.40 kN which is the least value of peak load among all the foam-filled tubes with cut-outs. The peak load reduction obtained for this configuration is 45.15% compared to peak load value of tube FP.

4.2 Energy absorption characteristics

It is observed from earlier research studies that the tubes with cut-outs yield lower peak load value but do not help in increasing the energy absorption of tube [27, 61]. Thus, an aluminium foam material is used in the present study to increase the energy absorption of the tubes with cut-outs. Foam filling has been done to observe the enhancement in the crashworthiness characteristics of tubes by increasing the energy absorption capacity of modified tube structure. When a foam-filled tube experiences axial compression, tube starts to buckle in a progressive crushing mode or concertina mode due to presence of cut-outs and foam will start to crush and will get filled in between the tube folds, thereafter reducing the displacement and increasing the resistance to deformation. Tube material attains plastic stage and deforms into fold. However, foam filled inside the tube attains its behaviour under plateau region where the load bearing capacity of the material increases gradually. This increase in the duration of one complete deformation fold and gradual increase in the load bearing capacity of material increases the area under load–displacement curve, which leads to increase in energy absorption capacity of the tube structure. Estimate of energy absorption capacity of tube can be made by calculating the area under the load–displacement profile of the tube while undergoing deformation. Figure 8 (a) and (b), 9 (a) and (b), and 10 (a) and (b) shows

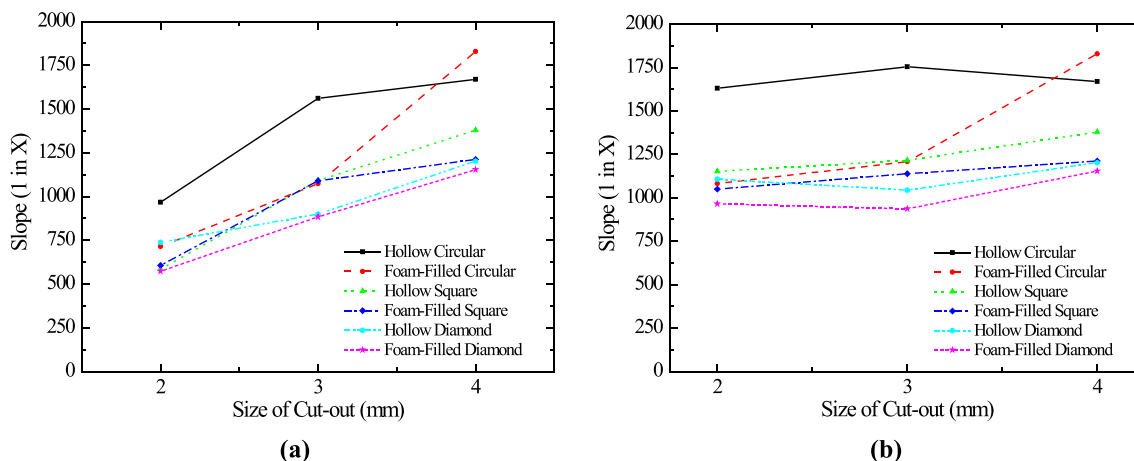


Fig. 13 Variation trend in slope of load–displacement curve for tube specimens with a Equal mass reduction criteria, and b equal net circumference criteria

the load–displacement profiles of all the tube configuration, and since the area under profile curve of foam-filled tube seems larger than the hollow tube for each of the configuration, thus it can be said that the foam filling in tubes has helped a to increase the energy absorption capacity of the tubes. For the negligible amount on increment in peak load value of foam-filled tubes, significant amount of increase is observed in their energy absorption capacity as compared to hollow tube configurations.

4.2.1 Energy absorption capacity of tubes

The foam-filled tube configurations with different shapes of cut-outs and having equal net circumference criteria, i.e. FP-C-2-6, FP-S-2-6, and FP-D-2-6, have yielded the energy absorption capacity of 11.7 J, 11.4 J, and 11.5 J, respectively. It can be seen from Tables 6, 7, and 8 that these configurations possess the highest energy absorption capacity as compared to their peer configurations of respective cut-out shapes. However, from Tables 6 and 8, in the case of hollow tubes with cut-outs, the highest amount of energy absorption is obtained in HP-S-2-6 tube configuration which is 10.8 J. This value is 19.4% less than the energy absorption value of hollow tube without cut-outs. But, in case of foam-filled tubes with cut-outs, the highest amount of energy absorption, i.e. 11.7 J, is obtained in FP-C-2-6 tube configuration which is 16.5% less than the energy absorption capacity of foam-filled tubes without any cut-outs.

Further, Figs. 14 and 15 illustrate the bar chart of energy absorbed by the hollow and foam-filled tubes with different shapes of cut-outs having the equal mass reduction criteria and equal net circumference criteria, respectively. On X-axis, tube specimens are mentioned with their cut-out size

and number. On Y-axis, energy absorption capacity of tube is plotted. From both the charts, it is observed that the foam filling in tubes has enhanced the energy absorption capacity of the modified tubes. In Fig. 14, the enhancement range of 4.6% to 15.5% has been achieved in the foam-filled modified tubes with equal mass reduction criteria as compared to hollow modified tubes. Maximum increase in energy absorption of 15.5% is observed in FP-C-3-5 tube specimen. However, the minimum increase in energy absorption of 4.6% is observed in FP-S-3-5 tube specimen. The increase in energy absorption is highest for the FP-S-2-12 configuration among all the other modified configurations.

In Fig. 15, the enhancement range of 5.26% to 14.41% has been attained in the foam-filled modified tubes with equal net circumference criteria. In this, the maximum and minimum increase in the energy absorption capacity is observed in the tube specimens FP-S-2-6 and FP-C-3-4, respectively, as compared to their hollow counterparts modified with cut-outs.

4.2.2 Interaction effect in the composites

This section deals with the investigation of the effect of foam filling in the hollow tubes and to understand the change in its deformation behaviour. This study has been carried out by investigating the interaction between the two different materials, i.e. AA6061-T6 tube and aluminium foam. The effect of interaction can be observed when the tube deforms into folds under compression and the foam inside the tube also compresses along with the tube. This filled foam will get compressed in the form of tube's internal structure during folding. Therefore, the deformation rate of tube folding will be much slower in

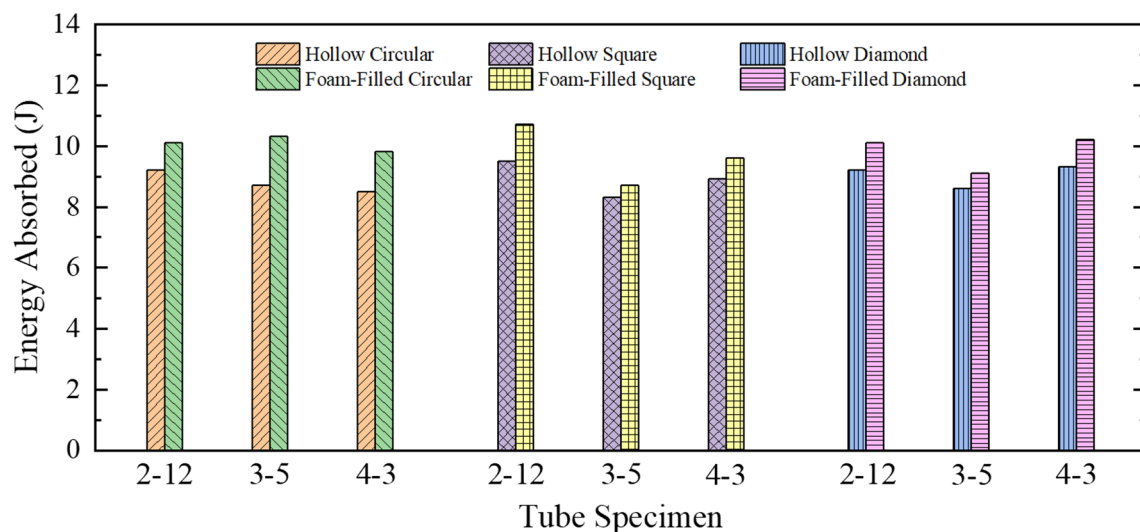


Fig. 14 Energy absorbed by tube specimens of equal mass reduction criteria

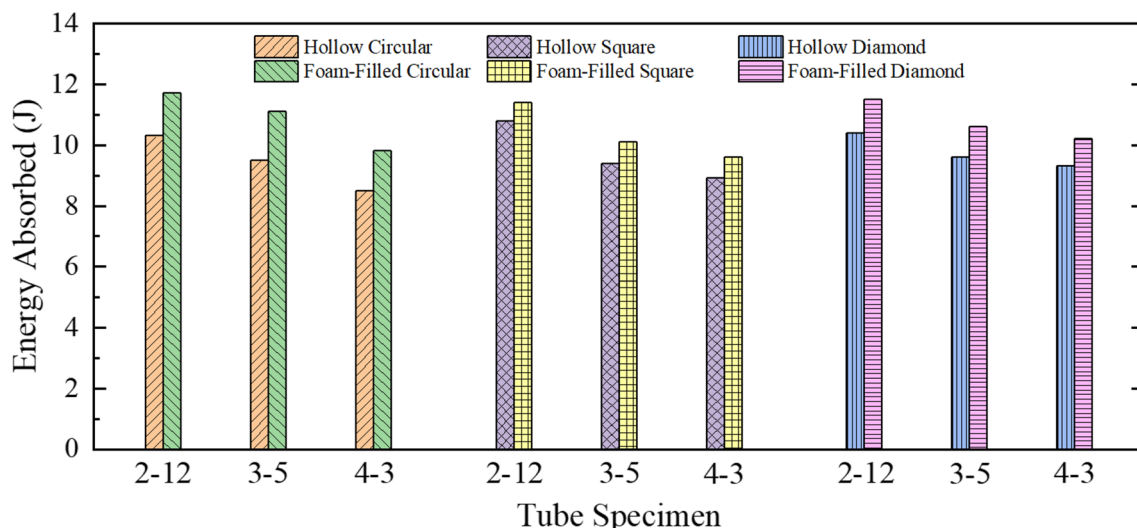


Fig. 15 Energy absorbed by tube specimens of equal net circumference criteria

case of foam-filled tube as compared to the hollow tube. This gradual deformation rate will increase the energy absorbed by the composite structure, i.e. foam-filled tube. Thus, increase in energy absorption capacity of the foam-filled tube structure will be an additional advantage to the modified tube structure provided with cut-outs and foam filling. The interaction effect can be studied by estimating the energy absorbed by these two materials individually and in-together. Energy absorbed due to interaction between two materials can be estimated as,

$$(E_{\text{absorbed}})_{\text{interact}} = (E_{\text{absorbed}})_{\text{FP}} - [(E_{\text{absorbed}})_{\text{HP}} + (E_{\text{absorbed}})_{\text{Foam}}] \tag{3}$$

In Eq. (3), $(E_{\text{absorbed}})_{\text{interact}}$ stands for the energy absorbed due to interaction effect between tube and foam material. It is the extra energy absorbed by the composite structure of foam-filled tube which cannot be absorbed by the two components individually. It can be termed as the interaction energy of the foam-filled tubes. $(E_{\text{absorbed}})_{\text{FP}}$, $(E_{\text{absorbed}})_{\text{HP}}$, and $(E_{\text{absorbed}})_{\text{Foam}}$ are the energy absorbed by the foam-filled tube, hollow tube and foam, respectively. Figure 16 represents the energy absorbed by the hollow tube, foam-filled tube, and the bare foam part, individually.

In order to further understand the interaction effect, another parameter, i.e. interaction ratio (IR) can be defined as,

$$\text{IR} = \frac{SEA_{\text{FP}} - (SEA_{\text{HP+Foam}})}{SEA_{\text{HP+Foam}}} \tag{4}$$

In Eq. (4), SEA_{FP} and $SEA_{\text{HP+Foam}}$ are the specific energy absorption of foam-filled tube and the sum of specific energy absorption of hollow tube and bare foam individually. Specific energy absorption (SEA) of any tube specimen can be calculated as the ratio of actual energy absorbed by the specimen to the mass of the specimen. $SEA_{\text{HP+Foam}}$ can be calculated as,

$$SEA_{\text{HP + Foam}} = \frac{(E_{\text{absorbed}})_{\text{HP}} + (E_{\text{absorbed}})_{\text{Foam}}}{M_{\text{HP}} + M_{\text{Foam}}} \tag{5}$$

In Eq. (5), M_{HP} and M_{Foam} are the mass of hollow tube and bare foam part, respectively.

Figure 16 (a) presents the comparison between energy absorbed by the foam-filled tube and the tube and foam separately. Energy absorbed by foam-filled tube is higher than the sum of energy absorbed by tube and foam individually. This extra amount of energy is absorbed due to the interaction between tube and foam. Figure 16 (b) shows the grey shaded region between the two curves which is the influence of interaction due to foam filling in hollow tube without cut-outs. Moreover, the interaction ratio (IR) for foam-filled tube (FP) is 2.74%, which shows the positive influence of foam filling on the energy absorption characteristics of tube.

Table 9 enlists the interaction ratio (IR) values for all the foam-filled tubes with cut-outs. The value of IR for each specimen is obtained as a positive value showing the positive influence of foam filling on the tube with all the three different shapes of cut-out. The present study has been carried out considering the single buckling response of tube under impact loading, and limiting the deformation length up to 30% of the

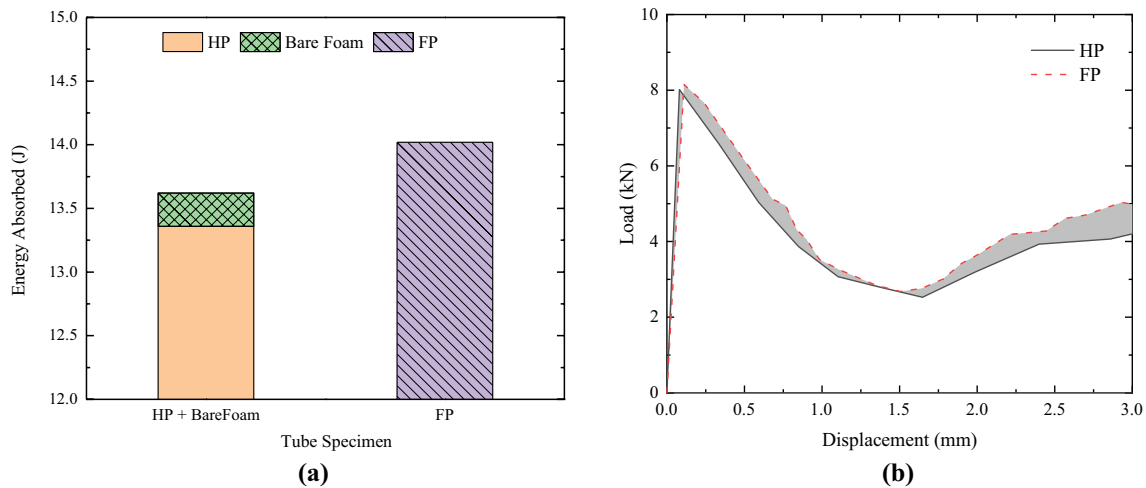


Fig. 16 **a** Energy absorption comparison and **b** interaction effect of hollow tube (HP), bare foam, and foam-filled tube (FP)

Table 9 Interaction ratio (IR) values of foam-filled tube specimens with cut-outs

Tube specimen	SEA_{FP}	$SEA_{HP+Foam}$	IR%
FP	12.79	12.45	2.74
FP-C-2-12	9.82	9.22	6.54
FP-C-3-5	9.99	8.65	15.50
FP-C-4-3	9.49	8.46	12.09
FP-C-2-6	10.94	9.86	10.91
FP-C-3-4	10.48	9.23	13.51
FP-S-2-12	10.38	9.41	10.37
FP-S-3-5	8.44	8.29	1.82
FP-S-4-3	9.29	8.86	4.96
FP-S-2-6	10.66	10.41	2.42
FP-S-3-4	9.58	9.16	4.64
FP-D-2-12	9.69	9.11	6.37
FP-D-3-5	8.78	8.53	2.91
FP-D-4-3	9.90	9.27	6.75
FP-D-2-6	10.74	9.97	7.76
FP-D-3-4	10.04	9.35	7.38

original tube length. Thus, the value of IR can show much effectiveness due to foam filling in multiple buckling response of tubes.

5 Conclusions

The present investigation is carried out to understand the deformation behaviour of thin-walled tubes subjected to impact loading. The comparison of tube buckling behaviour

is carried out in between tube without cut-outs and tubes with different shapes of cut-outs. Further, the tubes are filled with aluminium foam material and are compared with the behaviour of their hollow counterparts. This study has helped to understand the initial buckling behaviour of tube, during the formation of first fold, by estimating the parameters like load–displacement curve profile, variation of slope of the load–displacement profile, reduction in initial peak load value, energy absorption characteristics of tubes, and interaction effect between the tube and foam. Following are the conclusions drawn from the present investigation:

1. Significant load reduction has been reported when comparing tubes with and without cut-outs of various shapes. Furthermore, the new proposed cut-out designs, namely square and diamond shapes, demonstrated a greater reduction in peak load value than tubes with circular cut-outs. In terms of percentage, the maximum peak load reduction in tubes with circular form cut-outs is 42.3%, while the maximum reduction in tubes with square and diamond shape cut-outs is 46.54% and 47.69%, respectively. As a result, the lower the magnitude of peak load, the greater the peak load reduction and the lesser the force passed through the tube to its far end.
2. The variance in slope of the load–displacement curve profile is found to increase with the size of the cut-outs. To guarantee a progressive transfer rate of force through the tube, the slope of the load–displacement curve should be as small as possible. This will result in minimal jerks for the object or occupants.
3. The foam-filling technique in hollow tubes with cut-outs has resulted in the development of a novel tubular construction with numerous changes. Foam filling has

shown an increase in energy absorption capacity of tubes as well as an increase in energy efficiency of tubes up to 79.3%. This greatest gain in energy efficiency is almost 36.7% and 42.37% higher than the energy efficiency of foam-filled tubes without cut-outs and hollow tubes without cut-outs, respectively.

4. During deformation under impact loading, there is a significant interaction effect between the foam and the tube. The predicted interaction ratio based on the specific energy absorption capacity of foam-filled tubes with cut-outs and their hollow counterparts had a beneficial influence, with the most significant interaction ratios in foam-filled tubes with circular cut-outs.

Overall, this comprehensive study has provided a crucial insight in understanding the buckling behaviour of tube with different shapes of cut-outs under the influence of foam filled in tubes. From the present study, it can be said that tubes with square cut-outs have provided the most improved crashworthiness characteristics. However, estimations of an entire tube behaviour cannot be inferred just from the tube's initial buckling mode. Yet, it has significantly reduced the peak load and slope value of the load–displacement curve profile.

References

1. Pugsley A, Macaulay M (1960) The large-scale crumpling of thin cylindrical columns. *Q J Mech Appl Math* 13:1–9. <https://doi.org/10.1093/qjmam/13.1.1>
2. Alexander JM (1960) An approximate analysis of the collapse of thin cylindrical shells under axial loading. *Q J Mech Appl Math* 13:10–15. <https://doi.org/10.1093/qjmam/13.1.10>
3. Andrews KRF, England GL, Ghani E (1983) Classification of the axial collapse of cylindrical tubes under quasi-static loading. *Int J Mech Sci* 25:687–696. [https://doi.org/10.1016/0020-7403\(83\)90076-0](https://doi.org/10.1016/0020-7403(83)90076-0)
4. Abramowicz W, Jones N (1984) Dynamic axial crushing of square tubes. *Int J Impact Eng* 2:179–208. [https://doi.org/10.1016/0734-743X\(84\)90010-1](https://doi.org/10.1016/0734-743X(84)90010-1)
5. Abramowicz W, Jones N (1984) Dynamic axial crushing of circular tubes. *Int J Impact Eng* 2:263–281. [https://doi.org/10.1016/0734-743X\(84\)90010-1](https://doi.org/10.1016/0734-743X(84)90010-1)
6. Abramowicz W, Jones N (1986) Dynamic progressive buckling of circular and square tubes. *Int J Impact Eng* 4:243–270. [https://doi.org/10.1016/0734-743X\(86\)90017-5](https://doi.org/10.1016/0734-743X(86)90017-5)
7. Abramowicz W, Jones N (1997) Transition from initial global bending to progressive buckling of tubes loaded statically and dynamically. *Int J Impact Eng* 19:415–437. [https://doi.org/10.1016/S0734-743X\(96\)00052-8](https://doi.org/10.1016/S0734-743X(96)00052-8)
8. Reid SR (1993) Plastic deformation mechanisms in axially compressed metal tubes used as impact energy absorbers. *Int J Mech Sci* 35:1035–1052. [https://doi.org/10.1016/0020-7403\(93\)90054-X](https://doi.org/10.1016/0020-7403(93)90054-X)
9. Karagiozova D, Jones N (1992) Dynamic pulse buckling of a simple elastic-plastic model including axial inertia. *Int J Solids Structures* 29:1255–1272. [https://doi.org/10.1016/0020-7683\(92\)90236-M](https://doi.org/10.1016/0020-7683(92)90236-M)
10. Karagiozova D, Jones N (1992) Dynamic buckling of a simple elastic-plastic model under pulse loading. *Int J Non-Linear Mech* 27:981–1005. [https://doi.org/10.1016/0020-7462\(92\)90050-H](https://doi.org/10.1016/0020-7462(92)90050-H)
11. Karagiozova D, Jones N (2000) Dynamic elastic-plastic buckling of circular cylindrical shells under axial impact. *Int J Solids Struct* 37:2005–2034. [https://doi.org/10.1016/S0020-7683\(98\)00343-6](https://doi.org/10.1016/S0020-7683(98)00343-6)
12. Karagiozova D, Alves M, Jones N (2000) Inertia effects in axisymmetrically deformed cylindrical shells under axial impact. *Int J Impact Eng* 24:1083–1115. [https://doi.org/10.1016/S0734-743X\(00\)00028-2](https://doi.org/10.1016/S0734-743X(00)00028-2)
13. Karagiozova D, Jones N (2001) Influence of stress waves on the dynamic progressive and dynamic plastic buckling of cylindrical shells. *Int J Solids Struct* 38:6723–6749. [https://doi.org/10.1016/S0020-7683\(01\)00111-1](https://doi.org/10.1016/S0020-7683(01)00111-1)
14. Karagiozova D, Jones N (2001) Dynamic effects on buckling and energy absorption of cylindrical shells under axial impact. *Thin-Walled Struct* 39:583–610. [https://doi.org/10.1016/S0263-8231\(01\)00015-5](https://doi.org/10.1016/S0263-8231(01)00015-5)
15. Bhutada S, Goel MD (2022) Crashworthiness parameters and their improvement using tubes as an energy absorbing structure: an overview. *Int J Crashworthiness* 27:1569–1600. <https://doi.org/10.1080/13588265.2021.1969845>
16. Gupta NK, Gupta SK (1993) Effect of annealing, size and cut-outs on axial collapse behaviour of circular tubes. *Int J Mech Sci* 35:597–613. [https://doi.org/10.1016/0020-7403\(93\)90004-E](https://doi.org/10.1016/0020-7403(93)90004-E)
17. Arnold B, Altenhof W (2004) Experimental observations on the crush characteristics of AA6061 T4 and T6 structural square tubes with and without circular discontinuities. *Int J Crashworthiness* 9:73–87. <https://doi.org/10.1533/ijcr.2004.0273>
18. Arnold B, Altenhof W (2004) Finite element modeling of material damage in axially-loaded aluminum tubes with circular hole discontinuities. In: 8th International LS-DYNA Users Conference, Detroit, United States.
19. Cheng Q, Altenhof W, Li L (2006) Experimental investigations on the crush behaviour of AA6061-T6 aluminum square tubes with different types of through-hole discontinuities. *Thin-Walled Struct* 44:441–454. <https://doi.org/10.1016/j.tws.2006.03.017>
20. Han H, Cheng J, Taheri F, Pegg N (2006) Numerical and experimental investigations of the response of aluminum cylinders with a cutout subject to axial compression. *Thin-Walled Struct* 44:254–270. <https://doi.org/10.1016/j.tws.2005.11.003>
21. Cho YB, Bae CH, Suh MY, Sin HC (2006) A vehicle front frame crash design optimization using hole-type and dent-type crush initiator. *Thin-Walled Struct* 44:415–428. <https://doi.org/10.1016/j.tws.2006.03.011>
22. Shariati M, Rokhi MM (2008) Numerical and experimental investigations on buckling of steel cylindrical shells with elliptical cutout subject to axial compression. *Thin-Walled Struct* 46:1251–1261. <https://doi.org/10.1016/j.tws.2008.02.005>
23. Shariati M, Hatami H (2012) Experimental study of SS304L cylindrical shell with/without cutout under cyclic axial loading. *Theor Appl Fract Mech* 58:35–43. <https://doi.org/10.1016/j.tafmec.2012.02.005>
24. Hatami H, Shariati M (2017) Numerical and experimental investigation of SS304L cylindrical shell with cutout under uniaxial cyclic loading. *Iran J Sci Technol Trans Mech Eng* 43:139–153. <https://doi.org/10.1007/s40997-017-0120-2>
25. Song J, Guo F (2013) A comparative study on the windowed and multi-cell square tubes under axial and oblique loading. *Thin-Walled Struct* 66:9–14. <https://doi.org/10.1016/j.tws.2013.02.002>
26. Simhachalam B, Rao CL, Srinivas K (2014) Compression behavior and energy absorption of aluminum alloy aa6061 tubes with multiple holes. *Int J Comput Methods Eng Sci Mech* 15:232–241. <https://doi.org/10.1080/15502287.2014.882433>
27. Sankar HR, Parameswaran V (2016) Effect of multiple holes on dynamic buckling of stubby shells: an experimental and

- numerical investigation. *Int J Impact Eng* 96:129–145. <https://doi.org/10.1016/j.ijimpeng.2016.05.014>
28. Sankar HR, Parameswaran V (2018) Effect of circular perforations on the progressive collapse of circular cylinders under axial impact. *Int J Impact Eng* 122:346–362. <https://doi.org/10.1016/j.ijimpeng.2018.09.001>
 29. Rouzegar J, Assaei H, Elahi SM, Asiaei H (2018) Axial crushing of perforated metal and composite-metal tubes. *J Braz Soc Mech Sci Eng* 40:349. <https://doi.org/10.1007/s40430-018-1266-6>
 30. Özbek Ö, Bozkurt ÖY, Erklig A (2022) Development of a trigger mechanism with circular cut-outs to improve crashworthiness characteristics of glass fibre-reinforced composite pipes. *J Braz Soc Mech Sci Eng* 44:15. <https://doi.org/10.1007/s40430-021-03304-x>
 31. Taştan A, Acar E, Güler MA, Kılınçkaya Ü (2016) Optimum crashworthiness design of tapered thin-walled tubes with lateral circular cutouts. *Thin-Walled Struct* 107:543–553. <https://doi.org/10.1016/j.tws.2016.07.018>
 32. Nikkiah H, Guo G, Chew Y, Bai J, Song J, Wang P (2017) The effect of different shapes of holes on the crushing characteristics of aluminium square windowed tubes under dynamic axial loading. *Thin-Walled Struct* 119:412–420. <https://doi.org/10.1016/j.tws.2017.06.036>
 33. Nikkiah H, Baroutaji A, Olabi AG (2019) Crashworthiness design and optimisation of windowed tubes under axial impact loading. *Thin-Walled Struct* 142:132–148. <https://doi.org/10.1016/j.tws.2019.04.052>
 34. Kathiresan M (2020) Influence of shape, size and location of cut-outs on crashworthiness performance of aluminium conical frusta under quasi-static axial compression. *Thin-Walled Struct*. 154:106793. <https://doi.org/10.1016/j.tws.2020.106793>
 35. Taghipoor H, Eyvazian A, Ghiaskar A, Kumar AP, Hamouda AM, Gobbi M (2020) Experimental investigation of the thin-walled energy absorbers with different sections including surface imperfections under low-speed impact test. *Mater Today* 27:1498–1504. <https://doi.org/10.1016/j.matpr.2020.03.006>
 36. Reid SR, Reddy TY, Gray MD (1986) Static and dynamic axial crushing of foam-filled sheet metal tubes. *Int J Mech Sci* 28:295–322. [https://doi.org/10.1016/0020-7403\(86\)90043-3](https://doi.org/10.1016/0020-7403(86)90043-3)
 37. Hanssen AG, Langseth M, Hopperstad OS (2001) Optimum design for energy absorption of square aluminium columns with aluminium foam filler. *Int J Mech Sci* 43:153–176. [https://doi.org/10.1016/S0020-7403\(99\)00108-3](https://doi.org/10.1016/S0020-7403(99)00108-3)
 38. Gameiro CP, Carne J (2007) Dynamic axial crushing of short to long circular aluminium tubes with agglomerate cork filler. *Int J Mech Sci* 49:1029–1037. <https://doi.org/10.1016/j.ijmecsci.2007.01.004>
 39. Mirfendereski L, Salimi M, Ziaei-Rad S (2008) Parametric study and numerical analysis of empty and foam-filled thin-walled tubes under static and dynamic loading. *Int J Mech Sci* 50:1042–1057. <https://doi.org/10.1016/j.ijmecsci.2008.02.007>
 40. Abedi MM, Niknejad A, Liaghat GH (2012) Nejad MZ (2012) Theoretical and experimental study on empty and foam-filled columns with square and rectangular cross section under axial compression. *Int J Mech Sci* 65(1):134–146. <https://doi.org/10.1016/j.ijmecsci.2012.09.011>
 41. Cetin E, Baykasoğlu C (2019) Energy absorption of thin-walled tubes enhanced by lattice structures. *Int J Mech Sci* 157–158:471–484. <https://doi.org/10.1016/j.ijmecsci.2019.04.049>
 42. Gao Q, Liao WH (2021) Energy absorption of thin-walled tube filled with gradient auxetic structures-theory and simulation. *Int J Mech Sci* 201:106475. <https://doi.org/10.1016/j.ijmecsci.2021.106475>
 43. Magliaro J, Rahimidehgholam F, Altenhof W, Alpas AT (2023) Superior energy dissipation mechanisms compounded within composite AA6061/H130 foam structures. *Int J Mech Sci* 238:107843. <https://doi.org/10.1016/j.ijmecsci.2022.107843>
 44. Guo C, Mao J, Xie M (2022) Study on energy absorption characteristics of aluminium foam composite anti-collision rod. *J Braz Soc Mech Sci Eng* 44:266. <https://doi.org/10.1007/s40430-022-03577-w>
 45. Mohsenizadeh S, Ahmad Z, Alias A (2020) Numerical prediction on the crashworthiness of circular and square thin-walled tubes with polymeric auxetic foam core. *J Mater Eng Perform* 29:3092–3106. <https://doi.org/10.1007/s11665-020-04852-4>
 46. Mohammadi H, Ahmad Z, Petru M, Mazlan SA, Johari MAF, Hatami H, Kooloor SSR (2023) An insight from nature: honeycomb pattern in advanced structural design for impact energy absorption. *J Mater Res* 22:2862–2887. <https://doi.org/10.1016/j.jmrt.2022.12.063>
 47. Taghipoor H, Sefidi M (2022) Energy absorption of foam-filled corrugated core sandwich panels under quasi-static loading. *Proc Inst Mech Eng L: J Mater: Des Appl* 237:234–246. <https://doi.org/10.1177/14644207221110483>
 48. Montazeri S, Elyasi M, Moradpour A (2018) Investigating the energy absorption, SEA, and crushing performance of holed and grooved thin-walled tubes under axial loading with different materials. *Thin-Walled Struct* 131:646–653. <https://doi.org/10.1016/j.tws.2018.07.024>
 49. Goel MD (2016) Numerical investigation of the axial impact loading behaviour of single, double and stiffened circular tubes. *Int J Crashworthiness* 21:41–50. <https://doi.org/10.1080/13588265.2015.1113617>
 50. Estrada Q, Szwedowicz D, Rodriguez-Mendez A, Elías-Espinosa M, Silva-Aceves J, Bedolla-Hernández J, Gómez-Vargas OA (2019) Effect of radial clearance and holes as crush initiators on the crashworthiness performance of bi-tubular profiles. *Thin-Walled Struct* 140:43–59. <https://doi.org/10.1016/j.tws.2019.02.039>
 51. Pirmohammad S, Esmaeili-Marzdashti S (2019) Multi-objective crashworthiness optimization of square and octagonal bitubal structures including different hole shapes. *Thin-Walled Struct* 139:126–138. <https://doi.org/10.1016/j.tws.2019.03.004>
 52. Booth D, Kohar CP, Inal K (2021) Multi-objective optimization of a multi-cellular aluminium extruded crush rail subjected to dynamic axial and oblique impact loading conditions. *Thin-Walled Struct* 166:108021. <https://doi.org/10.1016/j.tws.2021.108021>
 53. Sarkhosh R, Farrokhabadi A, Zarei H (2022) Crashworthiness characteristics of composite cylindrical energy absorbers filled with honeycomb and foam under quasi-static load: experimental and analytical study. *J Braz Soc Mech Sci Eng* 44:346. <https://doi.org/10.1007/s40430-022-03662-0>
 54. Sarkabiri B, Jahan A, Rezvani MJ (2017) Crashworthiness multi-objective of the thin-walled grooved conical tubes filled with polyurethane foam. *J Braz Soc Mech Sci Eng* 39:2721–2734. <https://doi.org/10.1007/s40430-017-0747-3>
 55. Xie S, Zhang J, Liu X, Zheng S, Liu Z (2022) A reinforced energy-absorbing structure formed by combining multiple aluminium foam-filled open-hole tubes. *Int J Mech Sci* 224:107319. <https://doi.org/10.1016/j.ijmecsci.2022.107319>
 56. ABAQUS/Standard User's Manual, Version 6.14. Providence, RI: Dassault Systèmes Simulia Corp, 2014.
 57. Chen W, Song B (2011) Conventional Kolsky Bars. In: Chen W, Song B (eds) *Split Hopkinson (Kolsky) Bar - Design, Testing and Applications Mechanical Engineering Series*, © Springer Science+Business Media LLC. New York
 58. Johnson GR, Cook WH (1985) Fracture characteristics of three metals subjected to various strains, strain rates, temperatures and pressures. *Eng Fract Mech* 21:31–48. [https://doi.org/10.1016/0013-7944\(85\)90052-9](https://doi.org/10.1016/0013-7944(85)90052-9)

59. Goel MD, Matsagar VA, Gupta AK, Marburg S (2013) Strain rate sensitivity of closed cell aluminium fly ash foam. *Trans Non-ferrous Met Soc China* 23:1080–1089. [https://doi.org/10.1016/S1003-6326\(13\)62569-8](https://doi.org/10.1016/S1003-6326(13)62569-8)
60. Sinclair GB, Kondo M (1984) On the stress concentration at sharp re-entrant corners in plates. *Int J Mech Sci* 26:477–487. [https://doi.org/10.1016/0020-7403\(84\)90002-X](https://doi.org/10.1016/0020-7403(84)90002-X)
61. Bhutada S, Goel MD (2023) Progressive axial crushing behaviour of Al6061-T6 alloy tubes with geometrical modifications under impact loading. *Thin-Walled Struct* 182:110240. <https://doi.org/10.1016/j.tws.2022.110240>

Publisher's Note Springer Nature remains neutral with regard to jurisdictional claims in published maps and institutional affiliations.

Springer Nature or its licensor (e.g. a society or other partner) holds exclusive rights to this article under a publishing agreement with the author(s) or other rightsholder(s); author self-archiving of the accepted manuscript version of this article is solely governed by the terms of such publishing agreement and applicable law.